machines

MDPI

Article

Resonant Actuation Based on Dynamic Characteristics of Bistable Laminates

Yuting Liu [1], Jiaying Zhang [1,2,*], Diankun Pan [3], Zhangming Wu [3,4] and Qingyun Wang [1]

[1] School of Aeronautic Science and Engineering, Beihang University, Beijing 100191, China
[2] Ningbo Institute of Technology, Beihang University, Ningbo 315800, China
[3] Key Laboratory of Impact and Safety Engineering, Ningbo University, Ningbo 315211, China
[4] School of Engineering, Cardiff University, Cardiff CF24 3AA, UK
* Correspondence: jiaying.zhang@strath.ac.uk

Abstract: Bistable or multi-stable structures have found broad applications in the fields of adaptive structures, flow control, and energy harvesting devices due to their unique nonlinear characteristics and strong local stability behavior. In this paper, a theoretical model based on the principle of minimum potential energy and the Rayleigh–Ritz method is established to study the dynamic characteristics of a bistable unsymmetric laminate with a fixed center. Numerical results of this theoretical model were obtained and verified by an FEA model using ABAQUS. The nonlinear dynamic characteristics and the structural response under different levels of external excitation were investigated and verified by experiments. The realization conditions of single-well vibration and cross-well vibration of bistable laminates were determined, with which the actuation strategies can be optimized for targeting modal frequencies of bistable laminates.

Keywords: morphing structure; bistable composite laminate; non-linear dynamics; resonant actuation; snap-through

check for updates

Citation: Liu, Y.; Zhang, J.; Pan, D.; Wu, Z.; Wang, Q. Resonant Actuation Based on Dynamic Characteristics of Bistable Laminates. *Machines* **2023**, *11*, 318. https://doi.org/10.3390/machines11030318

Academic Editor: Jan Awrejcewicz

Received: 13 January 2023
Revised: 17 February 2023
Accepted: 17 February 2023
Published: 21 February 2023

1. Introduction

Adaptive structures have shown advantages in enhancing system functionality, reducing energy input, and adapting to various environment scenarios. Lightweight structures with high flexibility can be designed as adaptive structures, which have broad applications in the fields of space, wind turbines, flow control, energy harvesting devices, etc. Bistable and multi-stable structures are widely used to implement adaptive structures and systems due to their high structural utilization and shape adaptability. In recent years, in addition to morphing wings [1–3], bistable structures had been widely used in soft robots [4], energy harvesting devices [5,6], and large space deployable structures [7,8]. The stable configuration retaining ability and adjustable stiffness ability of bistable and multi-stable structures can highly improve their structural utilization efficiency. These advantages of bistable and multi-stable structures can reduce component complexity and remove unnecessary friction loss, which will benefit the engineering applications under frequently changing working conditions.

In 1981, Hyer [9] systematically and quantitatively studied the bistable characteristics of thin asymmetric composite laminates. The unique mechanical properties and potential application prospects of bistable structures has since attracted wide attention in research and industrial communities. In previous works, researchers have frequently established analytical models to predict the stable equilibrium state of bistable structures based on the principle of minimum potential energy, and derived the dynamical model based on the Hamilton principle. Hyer [10,11] introduced von Karman nonlinear terms into classical lamination theory and obtained analytical solutions for the cured shape of unsymmetric laminates, using the Rayleigh–Ritz method. Experimental results verify the analytical

model, which can accurately predict the cylindrical shapes of unsymmetric orthogonal laminates, as shown in Figure 1.

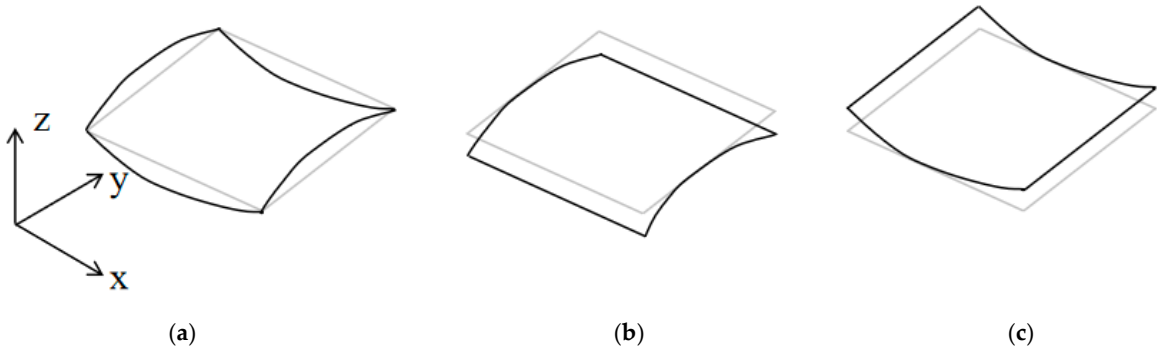

Figure 1. The configurations of a bi-stable cross-ply laminate. (**a**) Saddle-shaped configuration; (**b**) Cylindrical stable state A; (**c**) Cylindrical stable state B.

The prediction accuracy of stable configurations can be improved in several ways, such as by increasing the order of the admissible functions for the displacement and strain fields [12–15], and considering the influence of environmental parameters on laminates [16–18]. Previous research works on bistable laminates have had different focuses, such as the coupling effect between in-plane tension and transverse bending [19,20], the influence of different boundary conditions [21,22], and non-homogeneous curvature with the local edge effects [23,24]. Besides the traditional unsymmetric composite laminates, researchers have further studied new types of bistable laminates, such as prestressed laminate [25,26], variable stiffness laminate prestressing [27–29], hybrid laminate [30,31], and functional gradient material (FGM) laminate [32].

Due to their nonlinearity, bistable structures can rapidly transit between stable configurations, which is called the snap-through process. Different actuation methods can be used to trigger the progression from one stable state configuration to another, such as piezoelectric material MFC (macro-fiber composite) actuation, shape memory alloy actuation, thermal actuation, and magnetic actuation. Zhang et al. [33] fixed four vertices of the laminates and applied enough resultant force to generate large deformation. Schultz et al. [34] glued the MFC firmly to one side of the laminate, and applied a constant voltage to trigger one-way switching between the stable configurations. The theoretically predicted voltage of snap-through was consistent with the experimental testing results. Hufenbach et al. [35] attached SMA to laminates and used the residual stress after heating to obtain the snap-through behavior, however, it has been very difficult to establish a theoretical model for this mixed bistable structure. Dano et al. [36] installed SMA wires along the main curvature direction of laminates, and reported the convenience of using SMA wire to generate sufficient stress for actuation. Zhang et al. [37,38] investigated the dynamic behavior of a bistable beam actuated by SMA wires with varying external excitation. Experimental and simulation results both showed that bistable structures actuated by SMA wires performed well during the switching of bistable configurations. Brampton et al. [39] used aligned carbon plates as resistance heaters to heat bistable laminates, with the resultant thermal deformation able to trigger bistable configuration switching. Heating an electrothermal alloy embedded in the bistable laminate can also result in thermal deformation of the plate [40].

However, the resonance of bistable laminates can absorb energy to improve the actuation efficiency. Arrieta et al. [41] and Senda et al. [42] successively proposed a modal frequency-based strategy to generate sub-harmonic resonance by applying a harmonic voltage to the attached MFC of laminate. Experimental results showed that this method can reduce the required maximum excitation force but can only achieve one-way snap-through behavior. Senda et al. [42] increased the inertia of bistable composites by adding mass blocks, which significantly improved the actuation efficiency, however, this method introduces extra weight. Arrieta et al. [43] applied MFC to trigger cantilever laminates with

respect to different natural frequencies between stable configurations, to realize two-way snap-through behavior. Zhang et al. [44] studied the snap-through phenomenon and nonlinear vibration behavior of bistable laminates under shaker excitation, both theoretically and experimentally. In their theoretical model, the time-varying principal curvature was used to model the snap-through behavior of bistable laminates. It was shown that the maximum force required by dynamic actuation is much smaller than that of static actuation. Therefore, a dynamic-driven strategy for bistable structures with a focus on the first-order linear frequency is proposed.

In general, the bistable unsymmetric laminates have two stable configurations, stable configuration A and stable configuration B. As shown in Figure 2, the bistable structure has two local potential energy wells. Under external excitation, when the potential energy of the bistable structure is higher than the energy barrier between the two stable configurations, the snap-through occurs. The bistable laminate with unsymmetric diagram of potential wells can be designed by cutting and layering. Such bistable structures have two different stable configurations with different natural frequencies for each configuration. Therefore, stable configurations can be switched by changing the external excitation frequency.

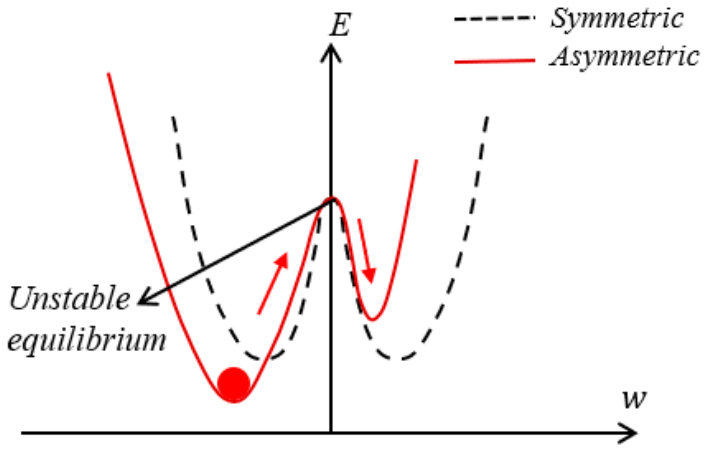

Figure 2. Potential energy diagrams of bistable unsymmetric structures.

The dynamic model of unsymmetric bistable laminates has been established with high computational efficiency and accuracy using the Rayleigh–Ritz method and the Hamilton principle, and the stretching–bending coupling was decoupled utilizing a membrane strain field. In this paper, the concept of resonance drive is proposed for the first time, and the realization conditions of the resonant actuation of laminates are accurately predicted by an analytical model, and experimentally verified by frequency sweeping and ABAQUS finite element software. Finally, using the simulation results obtained with the analytical model and the finite element models, the functionality of applying resonant actuation to achieve the snap-through was further verified experimentally. The resonant actuation strategy combines the inherent dynamic characteristics of the structures to enable efficient configuration switching, providing substantial potential for engineering applications of bistable structures.

2. Modeling

Resonant actuation is a new deformation mode proposed to minimize the actuation energy required to realize snap-through. The premise of achieving resonant actuation is to obtain the natural frequency of the stable configuration in the transverse direction. Therefore, it is necessary to establish an accurate analytical model to predict the modal frequency of laminates and then verify it experimentally and by finite element software such as ABAQUS.

2.1. The Finite Element Model

Only two stable configurations can be predicted by the finite element model. When the finite element model deforms freely, with the decrease of temperature the calculation results converge to the cylinder configuration curved along the length direction of the laminates. If the displacements of the vertices are constrained during the cooling process in the model, and the displacement constraints are removed in the subsequent analysis steps, the calculated results will converge to the cylinder configuration curved along the width direction of the laminates.

The stable configuration of bistable laminates is obtained by static analysis of two different boundary conditions. First of all, in the first "Static, General" analysis step, the laminated plate defines the range of temperature change in the predefined field. The model automatically converges to a stable configuration curved along the length of the laminate. Then, the calculation is restarted with a concentrated force applied to the four vertices along the out-of-plane direction while defining the temperature field in the first "Static, General" analysis step, removing the concentrated force in the second "static" analysis step. After the static analysis, two stable configurations of the bistable plate are obtained. The natural frequency of the bistable plate in the transverse direction is determined by the "Frequency" analysis step and the "Steady-state dynamics, Modal" step. On the basis of stable configuration, through the "Dynamic, Implicit" analysis step, the transverse acceleration excitation is applied to the midpoint of the laminates, and the steady-state response of the laminates is finally obtained.

The mechanical parameters of the material in this article are shown in Table 1.

Table 1. Material parameters of the bistable composite laminate.

Parameter	Value
Axial tensile modulus E_1/GPa	124.9
Transversal tensile modulus E_2/GPa	7.9
Shear modulus G_{12}/GPa	5.6
Shear modulus G_{23}/GPa	5.6
Poisson's ratio ν12	0.3
Longitudinal thermal expansion coefficient $\alpha_1/°C^{-1}$	4×10^{-7}
Transverse thermal expansion coefficient $\alpha_2/°C^{-1}$	1.8×10^{-5}
The thickness of layer t/mm	0.15

The shell element (S4R) in ABAQUS was used to establish the finite element model for rectangular orthogonal laminate layups. In our research, the temperature was set at 200°C in the initial analysis step. The temperature field was changed to 20 °C in the first static analysis step and the stable state A was obtained after the finite element model converged, as shown in Figure 3a. To obtain the stable state B, the first static analysis step is restarted, and the displacement perturbation along the z direction is applied to the four vertexes of the rectangle. The displacement perturbation is withdrawn in the second analysis step, and the model converged to the other configuration, stable state B, as shown in Figure 3b.

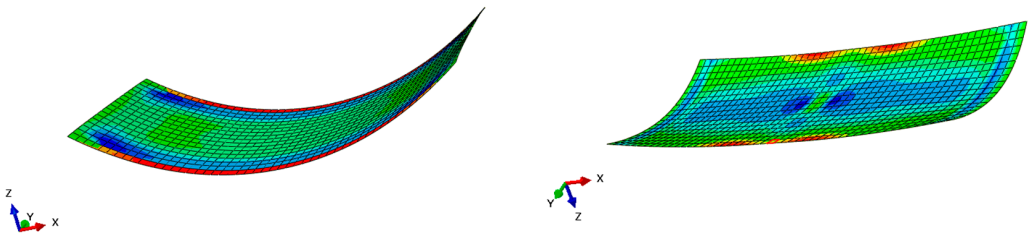

(**a**) (**b**)

Figure 3. The stable configuration of the bistable composite laminate: (**a**) stable state A; (**b**) stable state B.

2.2. The Static Behaviour of the Analytical Model

The dynamic model derived in this paper is analyzed using the Rayleigh–Ritz method and Hamilton's principle. In statics problems, the kinetic energy of the system is zero, and the potential energy is time-independent. The Lagrangian function in Hamilton's principle is defined as follows:

$$\begin{array}{l} L = T + W_F - \prod \\ \int_{t_0}^{t_1} L dt = 0 \end{array} \tag{1}$$

where T, W_F, and $\prod$ are the total kinetic energy, work done by external forces, and potential energy of the laminates, respectively.

Orthogonal bistable laminates have two cylindrical stable configurations and an unstable saddle configuration. A Cartesian coordinate system is established, with the origin of the coordinate system located at the center of the laminate, and the x and y axes parallel to the length and width of the rectangle, respectively. As the thickness of a bistable plate is much less than its length and width, the Kirchhoff hypothesis is applied. The strain of the laminate is:

$$\begin{bmatrix} \varepsilon_x \\ \varepsilon_y \\ \gamma_{xy} \end{bmatrix} = \begin{bmatrix} \varepsilon_x^0 \\ \varepsilon_y^0 \\ \gamma_{xy}^0 \end{bmatrix} + z \begin{bmatrix} k_x \\ k_y \\ k_{xy} \end{bmatrix} \tag{2}$$

where

$$\mathbf{k} = \begin{bmatrix} k_x \\ k_y \\ k_{xy} \end{bmatrix} = \begin{bmatrix} -\frac{\partial^2 w}{\partial x^2} \\ -\frac{\partial^2 w}{\partial y^2} \\ -2\frac{\partial^2 w}{\partial x \partial y} \end{bmatrix} \tag{3}$$

ε_x^0, ε_y^0, and γ_{xy}^0 are the mid-plane strains of the laminate, and $\mathbf{k}$ is the bending curvature and twisted curvature of the laminate.

Hyer [10] pointed out that in order to consider the large deformation of bistable laminates, nonlinear terms must be included in the geometric equation. According to the von Karman hypothesis, the relationship between in-plane strain and displacement in bistable laminates is given as:

$$\varepsilon^0 = \begin{bmatrix} \varepsilon_x^0 \\ \varepsilon_y^0 \\ \gamma_{xy}^0 \end{bmatrix} = \begin{bmatrix} \frac{\partial u^0}{\partial x} + \frac{1}{2}\left(\frac{\partial w}{\partial x}\right)^2 \\ \frac{\partial v^0}{\partial y} + \frac{1}{2}\left(\frac{\partial w}{\partial y}\right)^2 \\ \frac{\partial u^0}{\partial y} + \frac{\partial v^0}{\partial x} + \frac{\partial w}{\partial x}\frac{\partial w}{\partial y} \end{bmatrix} \tag{4}$$

where u^0, v^0, and w denote the in-plane displacement and out-of-plane displacement. Considering the residual thermal stress generated by the laminates during the curing process, and that there is no external energy input during the curing process, the total elastic potential energy of the laminates is given by the following formula:

$$\prod = \int_{-\frac{L_x}{2}}^{\frac{L_x}{2}} \int_{-\frac{L_y}{2}}^{\frac{L_y}{2}} \left(\frac{1}{2} \begin{bmatrix} \boldsymbol{\varepsilon}^{0\mathrm{T}} & \mathbf{k}^{\mathrm{T}} \end{bmatrix} \begin{bmatrix} \mathbf{A} & \mathbf{B} \\ \mathbf{B} & \mathbf{D} \end{bmatrix} \begin{Bmatrix} \boldsymbol{\varepsilon}^0 \\ \mathbf{k} \end{Bmatrix} - \begin{bmatrix} \mathbf{N}_S^{\mathrm{T}} & \mathbf{M}_S^{\mathrm{T}} \end{bmatrix} \begin{Bmatrix} \boldsymbol{\varepsilon}^0 \\ \mathbf{k} \end{Bmatrix} \right) \mathrm{dydx} \tag{5}$$

where L_x and L_y are the length and width of the rectangle, respectively, and are assumed to remain constant during the deformation process. **A**, **B**, and **D** are the stretching stiffness matrix, stretching–bending coupling stiffness matrix, and bending stiffness matrix, respectively. $\mathbf{N}_S$ and $\mathbf{M}_S$ are the resultant force and moment obtained by integrating the residual thermal stress in the thickness direction, and depend on the coefficient of thermal expansion of the plates.

However, if the bistable laminates are unsymmetric, stretching–bending coupling occurs. Therefore, the in-plane strain of laminates includes the membrane strain and the bending strain. Since the stretching stiffness matrix has no contribution to the origin

point of the coordinate in the thickness direction, the in-plane stress resultant is therefore expressed as:

$$\mathbf{N} = \mathbf{A}\boldsymbol{\varepsilon}^{\mathrm{m}} \tag{6}$$

The relationship between the in-plane strain and the membrane strain is expressed as:

$$\boldsymbol{\varepsilon}^{0} = \boldsymbol{\varepsilon}^{m} - \mathbf{A}^{-1}\mathbf{B}\mathbf{k} + \mathbf{A}^{-1}\mathbf{N}_{S}^{\mathrm{T}} \tag{7}$$

If the bending curvature $\mathbf{k}$ is not constant, the coupling term $\mathbf{A}^{-1}\mathbf{B}\mathbf{k}$ will contain the same unknown parameters caused by the out-of-plane displacement function w. The equation can be approximately decoupled through the method used by Ashton [45] in 1968 for the approximate solution of unsymmetric laminated plates:

$$\prod = \int_{-\frac{L_x}{2}}^{\frac{L_x}{2}} \int_{-\frac{L_y}{2}}^{\frac{L_y}{2}} \left(\frac{1}{2} \begin{bmatrix} \boldsymbol{\varepsilon}^{m\mathrm{T}} & \mathbf{k}^{\mathrm{T}} \end{bmatrix} \begin{bmatrix} \mathbf{A} & \mathbf{0} \\ \mathbf{0} & \mathbf{D} - \mathbf{B}\mathbf{A}^{-1}\mathbf{B} \end{bmatrix} \begin{Bmatrix} \boldsymbol{\varepsilon}^{m} \\ \mathbf{k} \end{Bmatrix} - \begin{bmatrix} \mathbf{N}_{S}^{\mathrm{T}} & \mathbf{M}_{S}^{\mathrm{T}} \end{bmatrix} \begin{bmatrix} \frac{1}{2}\mathbf{A}^{-1} & -\mathbf{A}^{-1}\mathbf{B} \\ \mathbf{0} & \mathbf{I} \end{bmatrix} \begin{Bmatrix} \mathbf{N}_{S} \\ \mathbf{k} \end{Bmatrix} \right) \mathrm{dydx} \tag{8}$$

If the bending curvature is constant, the theoretical model cannot accurately describe the deformation of laminates. Therefore, this paper assumes that the bending curvature of laminates is not constant. Considering the boundary conditions of laminates and the characteristics of symmetry and asymmetry of deformation, the fourth order out-of-plane displacement polynomial of laminates is assumed as:

$$w(t) = a(t)x^2 + a_1(t)y^2 + a_2(t)x^4 + a_3(t)y^4 + a_4(t)x^2y^2 \tag{9}$$

Assuming that the stretching membrane strain of laminates is related to the sectional shape of laminates and independent of the out-of-plane displacement function, the fourth order polynomial of the membrane strain is taken to be:

$$\begin{aligned} \varepsilon_x^m(t) &= b(t) + b_1(t)y^2 + b_2(t)y^4 + b_3(t)x^2y^2 \\ \varepsilon_y^m(t) &= c(t) + c_1(t)x^2 + c_2(t)x^4 + c_3(t)x^2y^2 \end{aligned} \tag{10}$$

where the unknown coefficients $a_i(t)$, $b_i(t)$, and $c_i(t)$ are generalized coordinates in the model. Therefore, the theoretical model of orthogonal unsymmetric laminates established in this paper has 13 unknown parameters.

For bistable laminates with a fixed center and free four edges, different external forces are applied to the four corners of the rectangle in the processes of curing and cooling. In this case, the work of external forces is expressed as:

$$W_F(t) = 2F\left(a(t)\left(\frac{L_x}{2}\right)^2 + a_1(t)\left(\frac{L_y}{2}\right)^2 + a_2(t)\left(\frac{L_x}{2}\right)^4 + a_3(t)\left(\frac{L_y}{2}\right)^4 + a_4(t)\left(\frac{L_x}{2}\right)^2\left(\frac{L_y}{2}\right)^2 \right) \tag{11}$$

where L_x, L_y and F denote plate length, width, and the concentrated force, respectively. The midpoint of the laminate is located at the origin of the coordinates, and the explicit time dependence has been omitted.

2.3. The Dynamic Behaviour of the Analytical Model

In the kinetic problem, the kinetic energy of the laminate is not zero and the potential energy varies with time. The analytical model simulates a bistable laminate with four free edges and its midpoint fixed on the shaker. In this paper, the influence of in-plane displacement field on kinetic energy is ignored, and the external displacement excitation applied by vibrator on laminates is $ws(t)$, sothe kinetic energy in this case is:

$$T = \frac{1}{2}\rho h \int_{-\frac{L_x}{2}}^{\frac{L_x}{2}} \int_{-\frac{L_y}{2}}^{\frac{L_y}{2}} \left(\frac{d(ws(t) + w(t))}{dt} \right)^2 dydx \tag{12}$$

Substitute the total kinetic energy, work done by external forces, and potential energy into Equation (1). According to the Hamilton principle, the variation of the Lagrangian function is equal to zero. Thirteen equations of motion are derived and expressed in the following matrix form:

$$\mathbf{M_1}\ddot{\mathbf{X}}_1 + \mathbf{D}\left(\dot{\mathbf{X}}_1\right) + \mathbf{K}_1(\mathbf{X}_1) = \mathbf{F}_1 \tag{13}$$

where $\mathbf{X}_1$ is the generalized displacement with 13 degrees of freedom, $\mathbf{M}_1$ is the mass matrix, $\mathbf{D}(\dot{\mathbf{X}}_1)$ is the damping force, $\mathbf{K}_1(\mathbf{X}_1)$ is the nonlinear stiffness force. $\mathbf{F}_1$ is the external force, which depends on the inertia and acceleration of the laminate.

To consider the damping effects in the model, the assumption of Rayleigh proportional damping is employed:

$$C(\dot{\mathbf{X}}_1, \mathbf{X}_1) = \alpha \mathbf{M}_1 \dot{\mathbf{X}}_1 + \beta \mathbf{K}_1(\mathbf{X}_1) \tag{14}$$

where α, β are the mass damping and stiffness damping coefficients, respectively. As the snap-through of bistable plates often occurs in low-frequency ranges, the contribution of stiffness damping is ignored. Therefore, it can be assumed that $\beta = 0$.

2.4. Prediction of Stable Configuration

In this section, an analytical model and a finite element model are described. The material parameters of the laminate are listed in Table 1, an 80 mm × 200 mm, $[0/90]_T$ laminate was selected. The accuracy of the analytical model was verified by comparing the out-of-plane displacement of the rectangular laminates. The comparison between the finite element results and the analytical prediction results of the stable configuration under different external forces is shown in Figure 4. It was found that the analytical model can provide satisfactory results compared with the finite element model, and slight error is reasonable.

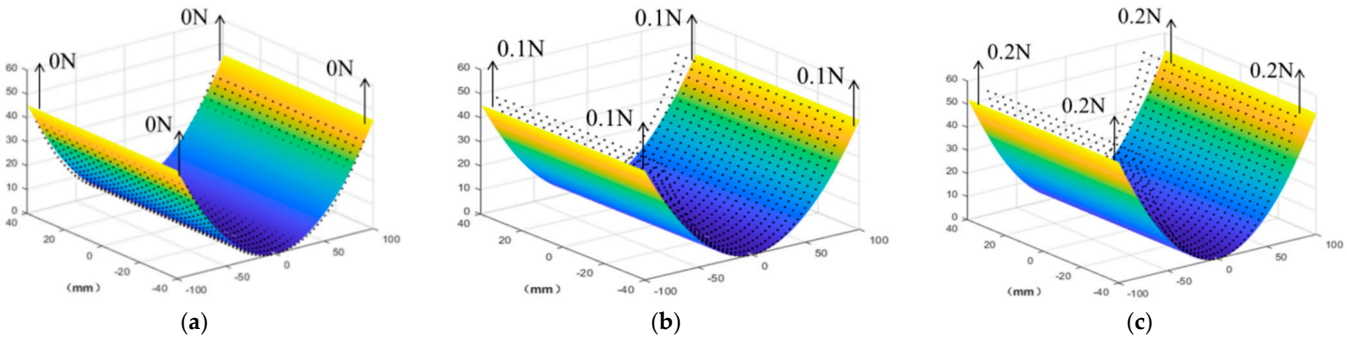

(**a**) (**b**) (**c**)

Figure 4. Predicted stable configurations of bistable laminates under different applied force, curved surface–theoretical results, discrete points–FEA. (**a**) 0 N; (**b**) 0.1 N; (**c**) 0.2 N.

The maximum out-of-plane displacements of bistable laminates under different external forces are shown in Table 2. When the external force is zero, the vertex displacement of the analytical model is larger than the finite element model. When the external force is not zero, the vertex displacement of the analytical model is reduced. The calculation errors of analytical models were less than 4% compared with the results given by the finite element models, attributed to fact that the curvature of the laminates and the strain distribution characteristics of the central plane were fully considered.

Table 2. Predicted out-of-plane deflection at the corners of the bistable plates.

Applied Force (N)	Analytical Model (mm)	Finite Element Model (mm)	Error
0	38.5675	37.3187	3.99%
0.1	45.3683	46.6199	2.68%
0.2	52.2781	53.3966	2.09%

In order to further verify the accuracy of the analytical model, the results of the analytical model were compared with the 3D scanning test, as shown in Figure 5. The black curved surface is the point-cloud image after scanning the test piece, the blank area is the marked points of the 3D scanning, and the discrete red points are the calculation results of the analytical model.

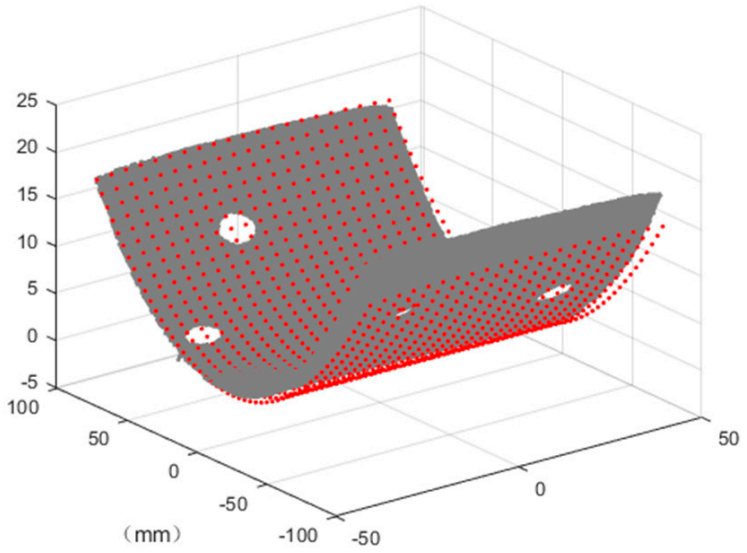

Figure 5. Deformation of the laminate, curved surface–3D scanning, discrete points–Analytical modal.

2.5. Geometric Parameter Analysis of Bistable Unsymmetric Laminates

The critical geometric conditions for the bistable properties of laminates were determined by varying the geometric parameters in the analytical model and the finite element model. With a 2.5 constant aspect ratio and allowing the length of laminates to vary continuously, the vertex-displacement bifurcation diagram for rectangular laminates with $[0/90]_T$ and $[0_2/90_2]_T$ layups in an ideal environment were analyzed and the results are shown in Figures 6 and 7.

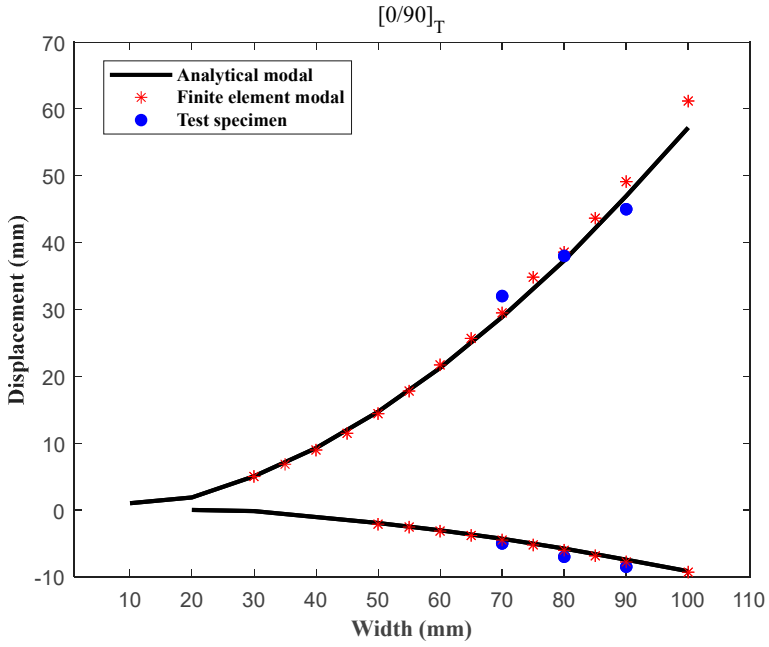

Figure 6. Bifurcation diagram of laminated plates with $[0/90]_T$ plies of different sizes.

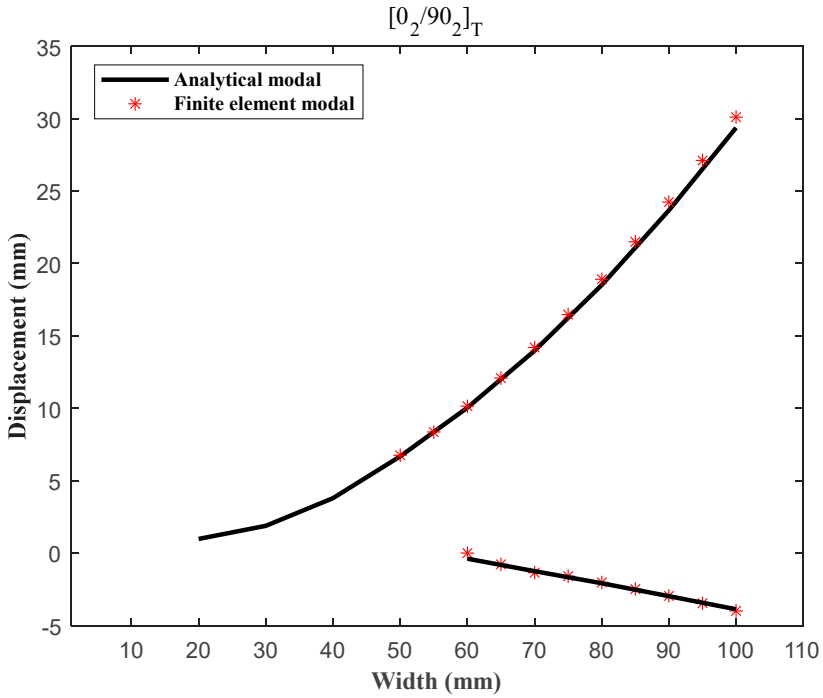

Figure 7. Bifurcation diagram of laminated plates with $[0_2/90_2]_T$ plies of different sizes.

The solid line represents the FEA simulation results and the red discrete points denote the prediction results of the analytical model. It can be seen that under ideal conditions the corner displacements of rectangular laminates $[0/90]_T$ and $[0_2/90_2]_T$ bifurcate with the increase of the side lengths of the laminates. Compared with the FEA results, the two methods were similarly successful in predicting the vertex displacement of the rectangular bistable laminates. Figure 6 shows that the FEA model predicted the bifurcation point of a $[0/90]_T$ laminate at around 30 mm. Figure 7 shows that the bifurcation point of the $[0_2/90_2]_T$ laminate predicted by FEA was 60 mm. The analytical model accurately predicted the bifurcation behavior of laminate with the increase of laminate size. The bistable critical length of laminates increased with the thickness. The FEA model is more accurate for predicting the bifurcation point, and the analytical model can not easily converge to a stable configuration when the width of the plate is near the bifurcation point.

The laminates with the $[0/90]_T$ layup were studied in the following experiments. Considering the avoidance of technical difficulties, to compare the theoretical and experimental results, three specimens with different dimensions were prepared. The vertex displacement is indicated by the discrete blue points in Figure 6, showing that the vertex displacements predicted by the theoretical model for the laminate in stable state B were in good agreement with the experimental results, while the errors for the stable state A were relatively large. The source of errors may be due to the use of inaccurate material parameters, the layering cooling process, defects in the test parts, and so on.

3. Kinetic Analysis

3.1. Fundamental Frequency Analysis

In order to obtain the resonant actuation conditions, the fundamental frequency of the laminates was first determined. The FEA model for the bistable laminate with a fixed center and four free edges was established in ABAQUS. In the analytical model, the damping coefficient was set to zero, and the laminate vibrates continuously in a simple harmonic motion. Through the free response curve of the vertex of stable state A in the analytical model, the first-order frequency of the bistable laminate under stable state A was obtained using fast Fourier transform. Three specimens were tested experimentally to obtain the free attenuation curve and the natural frequency using fast Fourier transform. Since the

damping ratio is sufficiently small, the natural frequency with damping is approximately equal to the natural frequency of the structure.

Figure 8 shows the natural frequencies of the laminated plates with different sizes. With the increase of laminate size, the first-order natural frequency of stable state A gradually decreased, and the rate of decrease tended to be gentle. For the natural frequency of the bistable laminate in stable state A, the finite element calculation results were in good agreement with the analytical solutions, but the experimental results were slightly lower in value than the theoretical results. Table 3 lists the first-order natural frequencies of rectangular laminates with different widths of 70 mm, 80 mm, and 90 mm, respectively. The results given by the finite element model were approximately consistent with the analytical solutions, while the first-order natural frequencies of the test specimens were smaller than both the FEM and analytical simulation results.

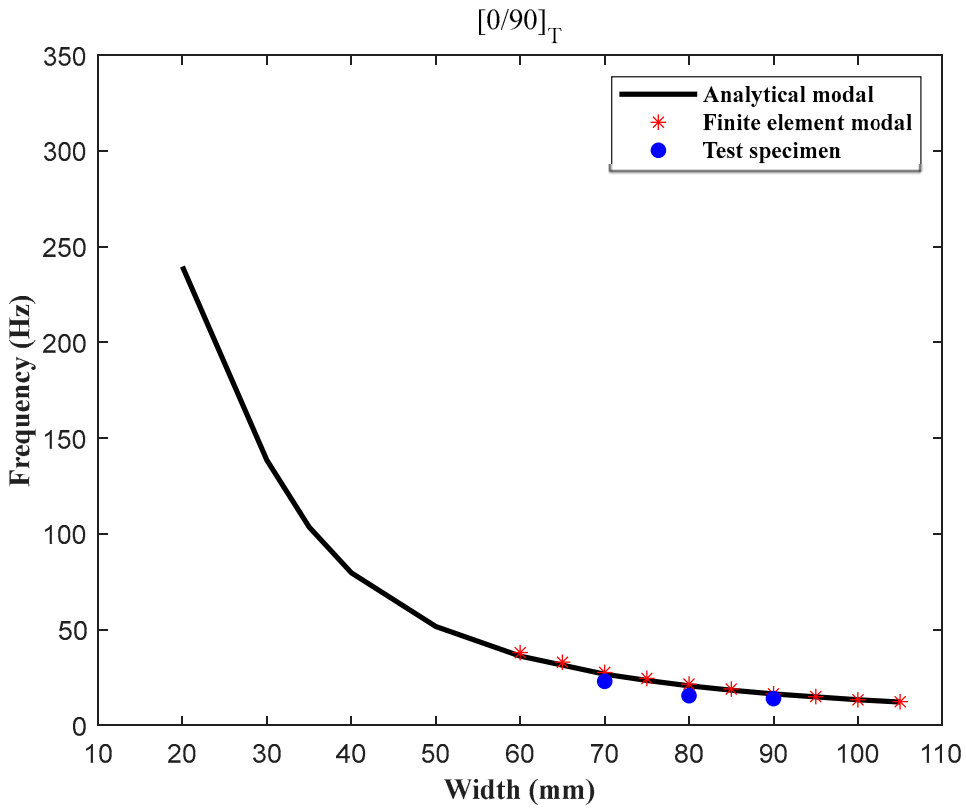

Figure 8. First-order natural frequencies of laminated plates of different sizes.

Table 3. First-order natural frequencies of laminated plates of different sizes.

Width (mm)	Analytical Model (Hz)	Finite Element Model (Hz)	Test Specimen (Hz)
70	26.77	27.6	23
80	20.649	21.5	15.5
90	16.4	16.5	14

Considering the difficulty of excitation conditions in the subsequent experiment, the rectangular laminates of 200 mm × 80 mm were selected for the resonance actuation.

3.2. Frequency Sweep Experiment

The main objective of this paper was to study the dynamic characteristics of bistable composite laminates actuated by resonance, which can provide a mechanical means for efficient actuation. This section investigates the dynamic responses of the 200 mm × 80 mm $[0/90]_T$ laminates under external excitation with different frequencies.

The nonlinear vibration of the bistable plate includes periodic vibration, quasi-periodic vibration, and chaotic vibration. When the excitation amplitude is small, the bistable composite laminates exhibit low-amplitude periodic vibration near the equilibrium configuration. When the excitation amplitude gradually increases, quasi-periodic vibration with a low amplitude is generated near the equilibrium configuration. When the amplitude is increased to a certain range, it results in chaotic motion with large amplitude between stable configurations, accompanied by single-well or cross-well snap-through.

The experimental device for carrying out the frequency-sweep experiment is illustrated in Figure 9. The sweep-signal generator transmits signals of different frequencies, which are amplified by the signal amplifier and stimulated by the shaker. At the same time, a laser rangefinder is used to record the dynamic response of a certain point on the laminate and a signal processor is used to record the response frequency.

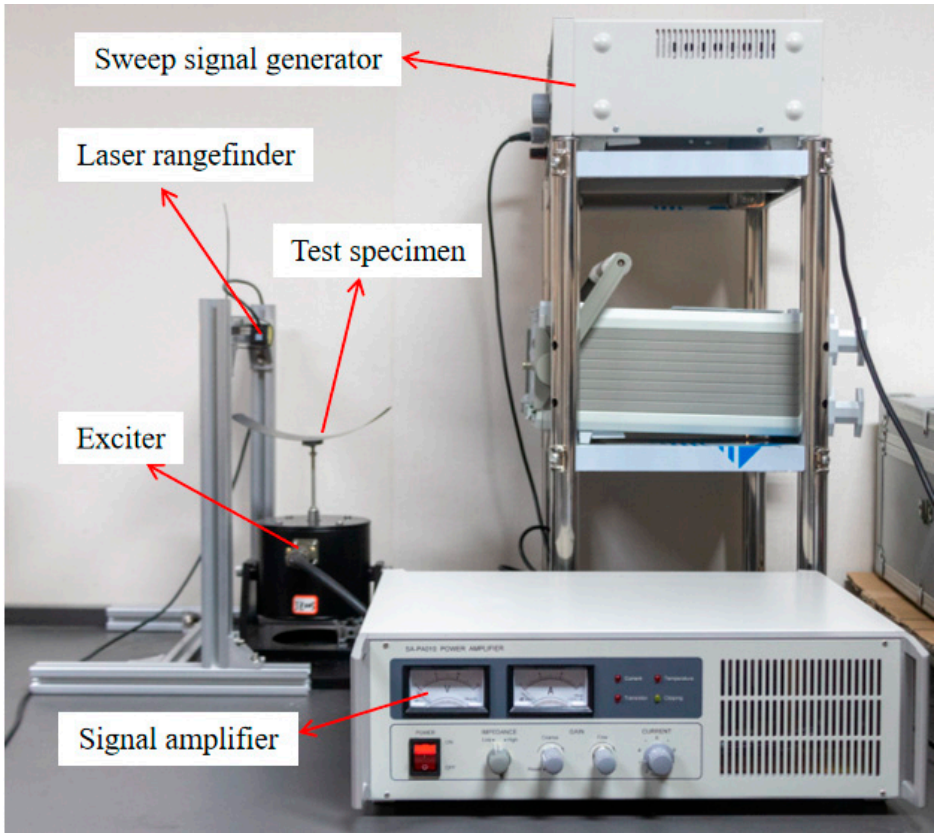

Figure 9. Diagram of the experimental apparatus for frequency-sweep experiment.

For the stable state A, the boundary conditions of the bistable laminate were a fixed center and four free edges, which were adapted to conduct the forward and reverse frequency-sweep experiment. The displacement curve of a certain point on the plate was recorded to obtain the frequency response curve of this point on the laminate. Under low-level amplitude excitation, the snap-through of the structure did not occur during the frequency sweep. In Figure 10, the solid black line denotes the result of the forward frequency-sweep experiment, while the dotted red line represents the result of reverse frequency-sweep experiment. The amplitude of the structure reached its maximum value near 15.6 Hz, which is the resonant frequency of the structure obtained in Section 3.1. Before the external excitation frequency reached 15.6 Hz, the response amplitude of the laminates increased. When the external excitation frequency reaches 15.6 Hz, the response amplitude decreased rapidly and then increased slowly. Because there was no snap-through, the frequency response curves of forward and reverse frequency sweeps show a consistent trend.

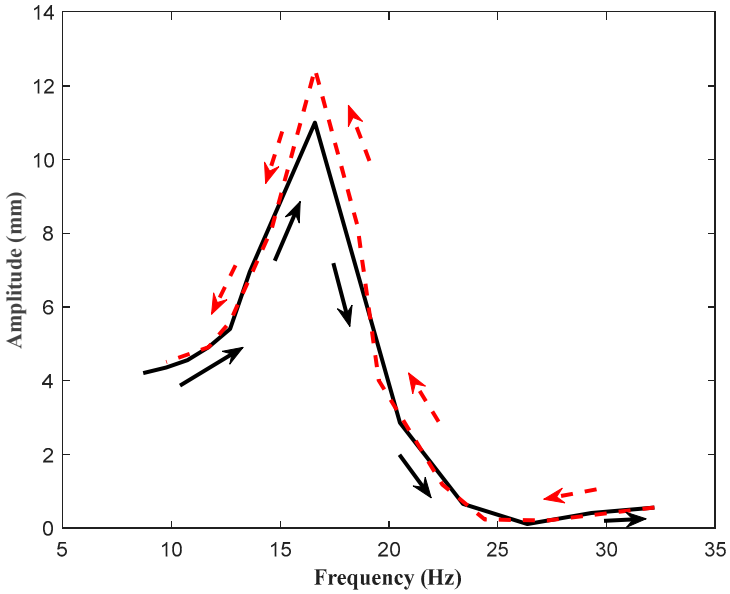

Figure 10. Vibration amplitudes of the bistable plates under low-level sinusoidal excitation at different frequencies.

The amplitude of the frequency sweep was further increased, and the dynamic response of laminates was recorded. The frequency response curve was obtained as shown in Figure 11. The solid line is the result of the forward frequency sweep and the dashed line is the result of the reverse frequency sweep. In the experiment, when the external excitation frequency of the structure was 15.6 Hz, the amplitude increased to the critical value, and the snap-through occurred. Subsequently, the laminate stabilized at the stable state B and continued to vibrate. Before the external excitation frequency reached 15.6 Hz, the response amplitude of the laminate gradually increased, reached the maximum value, and then changed suddenly. Finally, with the increase of excitation frequency, the response amplitude gradually decreased. Because the natural frequency of stable state B is high, the structure was always in stable state B when the frequency sweep was reversed. The response amplitude of stable state B increased with the decrease of the external excitation frequency.

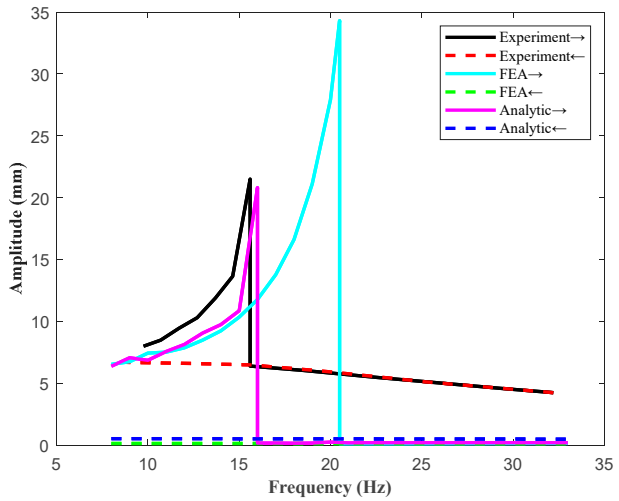

Figure 11. Vibration amplitudes of the bistable plates under higher-level sinusoidal excitation at different frequencies.

In the theoretical calculation, acceleration excitation, $as(t) = 60 \times \sin(2\pi\omega)$, is applied to the midpoint of the laminate. The critical amplitude of snap-through predicted by the finite element model was about 16 Hz, which is close to the experimental results but remarkably different from the natural frequency calculated in Section 3.1. The analytical model predicted that the snap-through amplitude is about 20.5 Hz, which is very close to the natural frequency calculated in Section 3.1. The coupling between the laminate and the shaker is not considered in the theoretical calculation, and the steady-state response amplitude of the stable state B after the snap-through was very small, close to 0. The stiffness of stable state B was relatively large, and the amplitude of steady-state response was small when the frequency was small.

4. Conclusions

The analytical model developed in this paper, applying a fourth-order displacement polynomial, can accurately predict the deformation of whole regions of bistable laminates without the limitations of single-point prediction. Compared with the finite element analysis, the analytical model dramatically simplified the process emlployed to predict convergent stable configuration. The natural frequency of the bistable laminate calculated by the analytical model was consistent with the FEA results. The deformation of laminates predicted by the FEA model and the analytical model was found to be in good agreement with the experiments. Due to inaccurate material parameters, the layup cooling process, defects in test parts, and other factors, there remain some inaccuracies in the analytical predictions of natural frequency.

The two stable configurations of the rectangular bistable laminates studied in this paper have different vibration modes. Under external excitation, the laminates can produce an approximate simple harmonic vibration response. A unidirectional snap-through occurs when the external excitation frequency is close to the natural frequency of the stable state A. Afterwards, the vibration continues until the stable state B is reached.

There are two basic vibration modes of bistable laminates under simple harmonic excitation: single-well vibration and cross-well vibration. Results show that the stiffness of stable state B in bistable laminates is larger than that of stable state A, so stable state B is less prone to snap-through. The snap-through behavior of laminate can be effectively controlled by changing the external excitation frequency. The experimental results show that the analytical model developed in this paper can accurately predict the dynamic characteristics of the bistable structural switching process, providing a theoretical model for the future study of the resonant actuation method.

Finally, the results of the sweep frequency experiment show that the frequency of the external harmonic load required for snap-through is in good agreement with the predicted natural frequency in chapter 3.1. This shows that the method is feasible to determine the realization conditions of resonant actuation. The frequency of the actuation load in the finite element model was also consistent with the predicted natural frequency. However, there remain large errors in the analytical model.

Author Contributions: Conceptualization, J.Z. and Y.L.; Methodology, J.Z. and Y.L.; Writing—original draft preparation, Y.L.; Review & editing, J.Z., D.P. and Z.W.; Supervision, J.Z. and Q.W. All authors have read and agreed to the published version of the manuscript.

Funding: This research was funded by the National Natural Science Foundation of China, grant number 12102017, the Research Fund of State Key Laboratory of Mechanics and Control of Mechanical Structures (Nanjing University of Aeronautics and Astronautics), grant number MCMS-E-0522G02 and the Fundamental Research Funds for the Central Universities, grant number YWF-22-L-1210.

Data Availability Statement: Not applicable.

Acknowledgments: This work is supported by the National Natural Science Foundation of China (Grant No. 12102017), the Research Fund of State Key Laboratory of Mechanics and Control of Mechanical Structures (Nanjing University of Aeronautics and Astronautics) (Grant No. MCMS-E-0522G02) and the Fundamental Research Funds for the Central Universities (YWF-22-L-1210).

Conflicts of Interest: The authors declare no conflict interest.

References

1. Zhang, J.; Shaw, A.D.; Wang, C.; Gu, H.; Amoozgar, M.R.; Friswell, M.I. Aeroelastic model and analysis of an active camber morphing wing. *Aerosp. Sci. Technol.* **2021**, *111*, 106534. [CrossRef]
2. Rivas-Padilla, J.R.; Boston, D.M.; Boddapati, K.; Arrieta, A.F. Topology Optimization and Experimental Validation of a Selectively Stiff Multistable Morphing Wing Section. In Proceedings of the AIAA SCITECH 2022 Forum, San Diego, CA, USA, 3–7 January 2022.
3. Rojas, S.; Riley, K.S.; Arrieta, A.F. Multistable bioinspired origami with reprogrammable self-folding. *J. R. Soc. Interface* **2022**, *19*, 20220426. [CrossRef]
4. Tang, Y.; Chi, Y.; Sun, J.; Huang, T.H.; Maghsoudi, O.H.; Spence, A.; Zhao, J.; Su, H.; Yin, J. Leveraging elastic instabilities for amplified performance: Spine-inspired high-speed and high-force soft robots. *Sci. Adv.* **2020**, *6*, eaaz6912. [CrossRef] [PubMed]
5. Lee, A.J.; Inman, D.J. A multifunctional bistable laminate: Snap-through morphing enabled by broadband energy harvesting. *J. Intell. Mater. Syst. Struct.* **2018**, *29*, 2528–2543. [CrossRef]
6. Lee, A.J.; Inman, D.J. Electromechanical modelling of a bistable plate with macro fiber composites under nonlinear vibrations. *J. Sound Vib.* **2019**, *446*, 326–342. [CrossRef]
7. Walker, M.G.; Seffen, K.A. On the shape of bistable creased strips. *Thin-Walled Struct.* **2018**, *124*, 538–545. [CrossRef]
8. Riemenschneider, J.; Pohl, M.; Ungurán, R.; Petrović, V.; Kühn, M.; Haldar, A.; Madhusoodanan, H.; Jansen, E.; Rolfes, R. Smart trailing edges for wind turbines. In *Smart Materials, Adaptive Structures and Intelligent Systems*; American Society of Mechanical Engineers: New York, NY, USA, 2018; Volume 51944, p. V001T04A001.
9. Hyer, M.W. Some observations on the cured shape of thin unsymmetric laminates. *J. Compos. Mater.* **1981**, *15*, 175–194. [CrossRef]
10. Hyer, M.W. Calculations of the Room-Temperature Shapes of Unsymmetric Laminates. *J. Compos. Mater.* **1981**, *15*, 296–310. [CrossRef]
11. Hyer, M.W. The Room-Temperature Shapes of Four-Layer Unsymmetric Cross-Ply Laminates. *J. Compos. Mater.* **1982**, *16*, 318–340. [CrossRef]
12. Jun, W.J.; Hong, C.S. Effect of residual shear strain on the cured shape of unsymmetric cross-ply thin laminates. *Compos. Sci. Technol.* **1990**, *38*, 55–67. [CrossRef]
13. Diaconu, C.G.; Weaver, P.M.; Arrieta, A.F. Dynamic analysis of bi-stable composite plates. *J. Sound Vib.* **2009**, *322*, 987–1004. [CrossRef]
14. Dano, M.L.; Hyer, M.W. Thermally-induced deformation behavior of unsymmetric laminates. *Int. J. Solids Struct.* **1998**, *35*, 2101–2120. [CrossRef]
15. Dano, M.L.; Hyer, M.W. Snap-through of unsymmetric fiber-reinforced composite laminates. *Int. J. Solids Struct.* **2002**, *39*, 175–198. [CrossRef]
16. Cho, M.; Kim, M.H.; Choi, H.S.; Chung, C.H.; Ahn, K.J.; Eom, Y.S. A study on the room-temperature curvature shapes of unsymmetric laminates including slippage effects. *J. Compos. Mater.* **1998**, *32*, 460–482. [CrossRef]
17. Etches, J.; Potter, K.; Weaver, P.; Bond, I. Environmental effects on thermally induced multistability in unsymmetric composite laminates. *Compos. Part A Appl. Sci. Manuf.* **2009**, *40*, 1240–1247. [CrossRef]
18. Gigliotti, M.; Jacquemin, F.; Molimard, J.; Vautrin, A. Transient and cyclical hygrothermoelastic stress in laminated composite plates: Modelling and experimental assessment. *Mech. Mater.* **2007**, *39*, 729–745. [CrossRef]
19. Reissner, E.; Stavsky, Y. Bending and stretching of certain types of heterogeneous aeolotropic elastic plates. *J. Appl. Mech.* **1961**, *28*, 402–408. [CrossRef]
20. Whitney, J.M.; Leissa, A.W. Analysis of heterogeneous anisotropic plates. *J. Appl. Mech.* **1969**, *36*, 261–266. [CrossRef]
21. Brunetti, M.; Mitura, A.; Romeo, F.; Warminski, J. Nonlinear dynamics of bistable composite cantilever shells: An experimental and modelling study. *J. Sound Vib.* **2022**, *526*, 116779. [CrossRef]
22. Brunetti, M.; Vidoli, S.; Vincenti, A. Bistability of orthotropic shells with clamped boundary conditions: An analysis by the polar method. *Compos. Struct.* **2018**, *194*, 388–397. [CrossRef]
23. Vidoli, S. Discrete approximations of the Föppl–von Kármán shell model: From coarse to more refined models. *Int. J. Solids Struct.* **2013**, *50*, 1241–1252. [CrossRef]
24. Brunetti, M.; Vincenti, A.; Vidoli, S. A class of morphing shell structures satisfying clamped boundary conditions. *Int. J. Solids Struct.* **2016**, *82*, 47–55. [CrossRef]
25. Fancey, K.S. Viscoelastically prestressed polymeric matrix composites: An overview. *J. Reinf. Plast. Compos.* **2016**, *35*, 1290–1301. [CrossRef]
26. Wang, B.; Ge, C.; Fancey, K.S. Snap-through behaviour of a bistable structure based on viscoelastically generated prestress. *Compos. Part B Eng.* **2017**, *114*, 23–33. [CrossRef]
27. Gürdal, Z.; Tatting, B.F.; Wu, C.K. Variable stiffness composite panels: Effects of stiffness variation on the in-plane and buckling response. *Compos. Part A Appl. Sci. Manuf.* **2008**, *39*, 911–922. [CrossRef]
28. Haldar, A.; Reinoso, J.; Jansen, E.; Rolfes, R. Snap-through of bistable configurations generated from variable stiffness composites. In *Multiscale Modeling of Heterogeneous Structures*; Springer: Cham, Swtizerland, 2018; pp. 61–82.
29. Haldar, A.; Reinoso, J.; Jansen, E.; Rolfes, R. Thermally induced multistable configurations of variable stiffness composite plates: Semi-analytical and finite element investigation. *Compos. Struct.* **2018**, *183*, 161–175. [CrossRef]

30. Chillara, V.S.C.; Dapino, M.J. Bistable morphing composites with selectively pre-stressed laminae. In Proceedings of the Behavior and Mechanics of Multifunctional Materials and Composites 2017, SPIE, Portland, OR, USA, 1 May 2017; Volume 10165, pp. 198–212.
31. Chillara, V.S.C.; Dapino, M.J. Stability considerations and actuation requirements in bistable laminated composites. *Compos. Struct.* **2018**, *184*, 1062–1070. [CrossRef]
32. He, X.Q.; Li, L.; Kitipornchai, S.; Wang, C.M.; Zhu, H.P. Bi-stable analyses of laminated FGM shells. *Int. J. Struct. Stab. Dyn.* **2012**, *12*, 311–335. [CrossRef]
33. Zhang, Z.; Wu, H.; He, X.; Wu, H.; Bao, Y.; Chai, G. The bistable behaviors of carbon-fiber/epoxy anti-symmetric composite shells. *Compos. Part B Eng.* **2013**, *47*, 190–199. [CrossRef]
34. Schultz, M.R.; Wilkie, W.K.; Bryant, R.G. Investigation of self-resetting active multistable laminates. *J. Aircr.* **2007**, *44*, 1069–1076. [CrossRef]
35. Hufenbach, W.; Gude, M.; Kroll, L. Design of multistable composites for application in adaptive structures. *Compos. Sci. Technol.* **2002**, *62*, 2201–2207. [CrossRef]
36. Dano, M.L.; Hyer, M.W. SMA-induced snap-through of unsymmetric fiber-reinforced composite laminates. *Int. J. Solids Struct.* **2003**, *40*, 5949–5972. [CrossRef]
37. Zhang, J.; Wu, Z.; Zhang, C.; Hao, L.; Nie, R.; Qiu, J. Nonlinear dynamics of shape memory alloys actuated bistable beams. *Smart Mater. Struct.* **2019**, *28*, 055009. [CrossRef]
38. Zhang, J.; Zhang, C.; Hao, L.; Nie, R.; Qiu, J. Exploiting the instability of Smart Structure for Reconfiguring. *Appl. Phys. Lett.* **2017**, *111*, 064102. [CrossRef]
39. Brampton, C.J.; Bowen, C.R.; Buschhorn, S.T.; Lee, J.; Pickering, S.G.; Wardle, B.L.; Kim, H.A. Actuation of bistable laminates by conductive polymer nanocomposites for use in thermal-mechanical aerosurface de-icing systems. In Proceedings of the 55th AIAA/ASMe/ASCE/AHS/SC Structures, Structural Dynamics, and Materials Conference, National Harbor, MD, USA, 13–17 January 2014; p. 0105.
40. Li, H.; Dai, F.; Du, S. The morphing bi-stable glass fiber–reinforced polymer laminates actuated by embedded electrothermal alloy. *J. Intell. Mater. Syst. Struct.* **2015**, *26*, 69–78. [CrossRef]
41. Arrieta, A.F.; Neild, S.A.; Wagg, D.J. Nonlinear dynamic response and modeling of a bi-stable composite plate for applications to adaptive structures. *Nonlinear Dyn.* **2009**, *58*, 259–272. [CrossRef]
42. Senba, A.; Ikeda, T.; Ueda, T. A two-way morphing actuation of bi-stable composites with piezoelectric fibers. In Proceedings of the 51st AIAA/ASME/ASCE/AHS/ASC Structures, Structural Dynamics, and Materials Conference 18th AIAA/ASME/AHS Adaptive Structures Conference, Orlando, FL, USA, 12–15 April 2010; p. 2744.
43. Arrieta, A.F.; Bilgen, O.; Friswell, M.I.; Hagedorn, P. Dynamic control for morphing of bi-stable composites. *J. Intell. Mater. Syst. Struct.* **2013**, *24*, 266–273. [CrossRef]
44. Zhang, W.; Liu, Y.Z.; Wu, M.Q. Theory and experiment of nonlinear vibrations and dynamic snap-through phenomena for bi-stable asymmetric laminated composite square panels under foundation excitation. *Compos. Struct.* **2019**, *225*, 111140. [CrossRef]
45. Ashton, J.E. Approximate solutions for unsymmetrically laminated plates. *J. Compos. Mater.* **1969**, *3*, 189–191. [CrossRef]